Phosphorylation of human aquaporin 2 (AQP2) allosterically controls its interaction with the lysosomal trafficking protein LIP5

Jennifer Virginia Roche[‡], Sabeen Survery[‡], Stefan Kreida[‡], Veronika Nesverova[‡], Henry Ampah-Korsah[‡], Maria Gourdon[‡], Peter M. T. Deen[§], and ![ORCID] Susanna Törnroth-Horsefield[‡1]

From the [‡]Department of Biochemistry and Structural Biology, Lund University, 221 00 Lund, Sweden and the [§]Department of Physiology, Radboud University Medical Center, 6525 GA Nijmegen, The Netherlands

Edited by Thomas Söllner

The interaction between the renal water channel aquaporin-2 (AQP2) and the lysosomal trafficking regulator-interacting protein LIP5 targets AQP2 to multivesicular bodies and facilitates lysosomal degradation. This interaction is part of a process that controls AQP2 apical membrane abundance in a vasopressin-dependent manner, allowing for urine volume adjustment. Vasopressin regulates phosphorylation at four sites within the AQP2 C terminus (Ser[256], Ser[261], Ser[264], and Thr[269]), of which Ser[256] is crucial and sufficient for AQP2 translocation from storage vesicles to the apical membrane. However, whether AQP2 phosphorylation modulates AQP2-LIP5 complex affinity is unknown. Here we used far-Western blot analysis and microscale thermophoresis to show that the AQP2 binds LIP5 in a phosphorylation-dependent manner. We constructed five phospho-mimicking mutants (S256E, S261E, S264E, T269E, and S256E/T269E) and a C-terminal truncation mutant (ΔP242) that lacked all phosphorylation sites but retained a previously suggested LIP5-binding site. CD spectroscopy indicated that wild-type AQP2 and the phospho-mimicking mutants had similar overall structure but displayed differences in melting temperatures possibly arising from C-terminal conformational changes. Non-phosphorylated AQP2 bound LIP5 with the highest affinity, whereas AQP2-ΔP242 had 20-fold lower affinity as determined by microscale thermophoresis. AQP2-S256E, S261E, T269E, and S256E/T269E all had reduced affinity. This effect was most prominent for AQP2-S256E, which fits well with its role in apical membrane targeting. AQP2-S264E had affinity similar to non-phosphorylated AQP2, possibly indicating a role in exosome excretion. Our data suggest that AQP2 phosphorylation allosterically controls its interaction with LIP5, illustrating how altered affinities to interacting proteins form the basis for regulation of AQP2 trafficking by post-translational modifications.

This article contains supplemental Table S1 and Figs. S1–S7.

[1] To whom correspondence should be addressed: Dept. of Biochemistry and Structural Biology, Lund University, P.O. Box 124, 221 00 Lund, Sweden. Tel.: 46-46-222-45-84; Fax: 46-46-222-41-16; E-mail: susanna.horsefield@biochemistry.lu.se.

The human body controls blood volume and osmolality by the vasopressin-dependent trafficking of aquaporin-2 (AQP2)[2] water channels to the apical membrane of the collecting duct principal cells (1). AQP2 trafficking involves a dynamic equilibrium between regulated exocytosis and endocytosis of AQP2-containing storage vesicles. During dehydration, vasopressin, released from the pituitary gland, binds to the V2 receptor in the basolateral membrane and triggers a cAMP signaling cascade. This ultimately results in fusion of AQP2-containing storage vesicles with the apical membrane as well as increased AQP2 membrane retention and elevated water reabsorption from pro-urine (2–4). After restoration of the dehydration, the reduced vasopressin levels lead to the internalization of AQP2 through endocytosis, after which it is stored in intracellular vesicles for another round of activation, degraded in lysosomes or released as exosomes (5, 6).

Multiple post-translational modifications within the AQP2 C terminus regulate its subcellular localization. In human AQP2, four phosphorylation sites have been identified: Ser[256], Ser[261], Ser[264], and Thr[269] (Ser[269] in mice), all of which are phosphorylated in a vasopressin-dependent manner (2–4, 7–9) (Fig. 1). Studies in mammalian cells, primarily using kinase and phosphatase inhibitors/activators, as well as phospho-mimicking mutants, have shown that Ser[256] plays the most prominent role: its phosphorylation by PKA is essential and sufficient for vasopressin-mediated translocation of AQP2 from storage vesicles to the apical membrane (2–4). Vasopressin also stimulates additional phosphorylation at Thr[269], and this has been shown to reduce the internalization rate, prolonging the time AQP2 resides in the apical membrane (8, 10, 11). The role of vasopressin-mediated phosphorylation of Ser[264] is unknown but has been suggested to play a role in AQP2 sorting within the endosomal system and may be involved in transcytosis from the basolateral membrane (7). In contrast, vasopressin triggers dephosphorylation of Ser[261], and AQP2 mimicking phosphorylation on Ser[261] only mainly resides in intracellular vesicles (12, 13). AQP2 endocytosis is enhanced by ubiquitination at
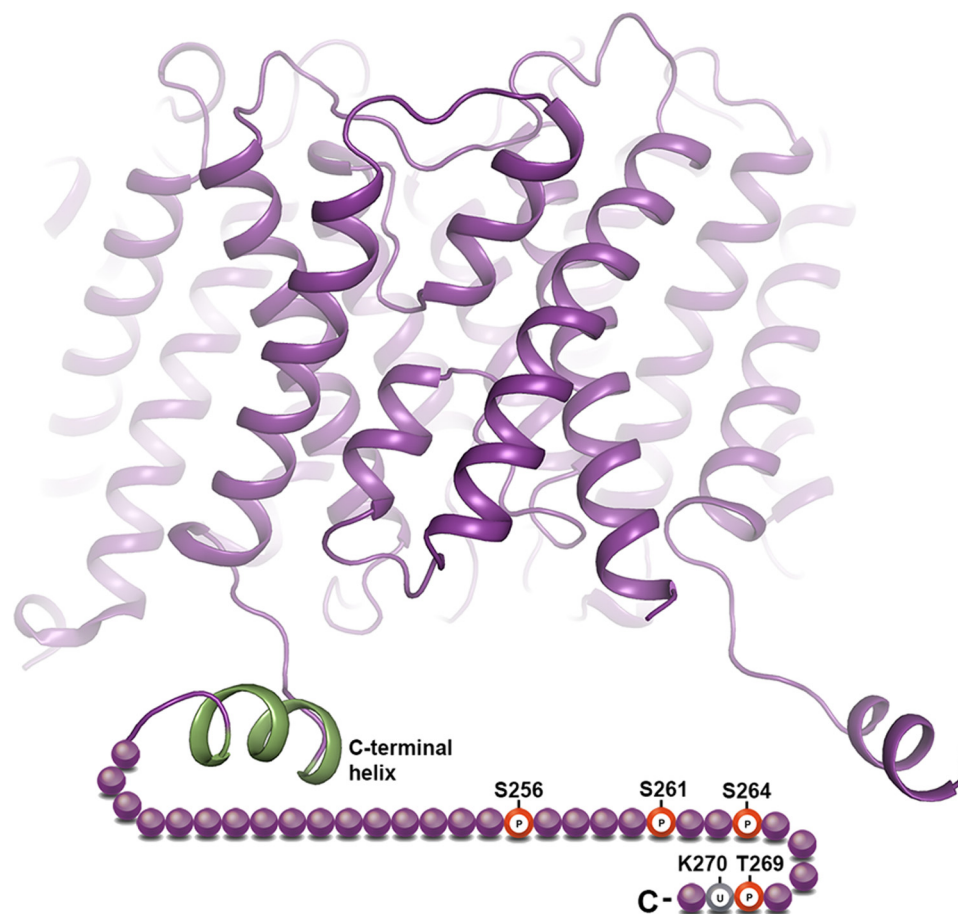
Figure 1. Crystal structure of human AQP2. Cartoon representation of the 2.75 Å human AQP2 crystal structure (Protein Data Bank code 4NEF) with residues that could not be resolved displayed as beads. Phosphorylation and ubiquitination sites are highlighted in *red* and *gray*, respectively. The proximal part of the C terminus that has been shown to bind LIP5 (20) forms a short helix (*green*).

Lys[270], which, when sustained, results in sorting into multivesicular bodies (MVBs) and subsequent lysosomal degradation (5). Interestingly, phosphorylation of Thr[269] is able to override the ubiquitin-internalization signal (8), and phosphorylation of Ser[261] has been shown to increase ubiquitinated AQP2 levels (13). This suggests that there is an intricate cross-talk between the post-translational modifications that determine AQP2 apical membrane abundance.

Membrane protein translocation between cellular compartments depends on the interaction with proteins of the membrane protein sorting and vesicular trafficking machinery. These interactions are governed by sorting signals within the membrane protein themselves, such as short linear sequences or post-translational modifications (14, 15). A number of proteins have been shown to interact with AQP2 and affect its cellular localization, including members of the 70-kDa heat shock protein family (Hsc70 and Hsp70) (16, 17), Annexin II (18), SPA-1 (the protein encoded by the signal-induced proliferation-associated gene-1) (19), and LIP5 (the lysosomal trafficking regulator (LYST)-interacting protein 5) (20). Several AQP2-interacting proteins have been shown to preferentially interact with non-phosphorylated or phosphorylated AQP2 (11, 21, 22). It is therefore plausible that altered affinities to interacting proteins form the rationale for how AQP2 phosphorylation determines its subcellular localization.

LIP5 plays an important role in MVB biogenesis where its interaction with components of the endosomal sorting complex required for transport (ESCRT)-III complex and the VPS4 ATPase helps coordinate membrane fission and ESCRT-III complex disassembly (23–25). Interestingly, LIP5 has also been shown to interact with membrane protein cargo, one of which is AQP2, thereby leading to its increased lysosomal degradation (20). Van Balkom *et al.* (20) demonstrated that LIP5 binds to the proximal part of the AQP2 C terminus, corresponding to a short C-terminal helix in its crystal structure (Fig. 1) (26), and that the interaction occurred regardless of the AQP2 phosphorylation and ubiquitination status. However, because the interaction was not further quantified, it is not known whether post-translational modifications of AQP2 result in modulation of the AQP2-LIP5 complex affinity.

In this work, we investigated the effect of AQP2 phosphorylation on the AQP2-LIP5 interaction in a quantitative manner. To do this, we constructed phospho-mimicking mutants of human AQP2 where the phosphorylated serine/threonine is replaced by glutamate, a substitution that is commonly used as a phospho-mimic (27). In addition to the single mutants S256E, S261E, S264E, and T269E, we also made a S256E/T269E double mutant, because phosphorylation of Thr[269] follows that of Ser[256]. The interaction with LIP5 was studied using far-Western blot and microscale thermophoresis (MST), revealing that
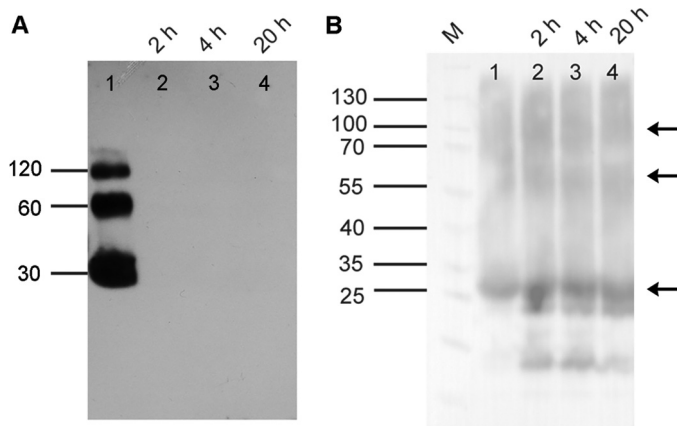
Figure 2. Phosphorylation of AQP2 in *P. pastoris*. *A*, purified AQP2 produced in *P. pastoris* was transferred to a PVDF membrane and probed for phosphorylation using Phos-tag BTL-111. A clear phosphorylation signal is seen for non-treated AQP2 (*lane 1*) with bands corresponding to monomeric (30 kDa), dimeric (60 kDa), and tetrameric (120 kDa) forms of the protein. Following treatment with alkaline phosphatase for 2, 4, and 20 h (*lane 2-4*), no bands can be seen, illustrating complete removal of phosphorylation. *B*, Western blot stained with antibody against the His tag shows that equal amount of AQP2 is present in all samples. Protein bands corresponding to those seen in *A* are marked with *arrows*. Protein masses are indicated in kDa.

although all AQP2 phosphorylation mutants were able to bind LIP5, there was a significant effect on the affinity, with four of five mutants having a higher K_d, as determined by MST. We further show that although the distal part of the C terminus that contains the phosphorylation sites was not critical for the AQP2-LIP5 interaction, removal of this region resulted in 20-fold lower affinity. This suggests that the distal AQP2 C terminus and its phosphorylation status plays an important role in modulating the affinity to LIP5, thereby fine-tuning its sorting into MVBs.

Results

Human AQP2 is phosphorylated when produced in Pichia pastoris

Wild-type human AQP2, AQP2 phospho-mimicking mutants (S256E, S261E, S264E, and T269E), and AQP2 truncated after Pro[242] (AQP2-ΔP242) were cloned into yeast expression vectors, overproduced in the yeast *P. pastoris*, and purified. Because *P. pastoris* is known to be able to phosphorylate recombinant proteins, including aquaporins (28), we decided to investigate whether this also holds true for human AQP2. Purified human AQP2 was run on an SDS-PAGE and probed for phosphorylation using Phostag[TM]-BTL-111. As seen in Fig. 2*A* (*lane 1*), a clear signal for phosphorylation is evident for AQP2. Three bands are observed, presumably corresponding to the AQP2 monomer, dimer, and tetramer. Three main bands are also seen in a Western blot stained with antibodies against the His tag (Fig. 2*B*), confirming their identity as AQP2. The apparent lower molecular mass for these bands compared with what is expected is a common phenomenon during SDS-PAGE analysis of membrane proteins (29).

The AQP2 phosphorylation status was further examined using mass spectrometry, whereby purified AQP2 was subjected to trypsin digestion and the peptides were analyzed by ESI-Orbitrap. Forty unique peptides could be assigned, corresponding to 38% of the amino acid sequence (Table 1). Phosphorylation was detected for nine of these unique peptides. Further MS/MS analysis revealed phosphorylation at three of four sites: Ser[256], Ser[261], and Ser[264]. Data from two representative MS/MS analyses, unambiguously assigning these phosphorylations by detecting an extra mass of 98 Da, are listed in supplemental Table S1 (mass errors displayed in supplemental Fig. S1). In the peptide [253]R.RQSVELHSPQSLP.R[268], all three serines were observed to be phosphorylated at the same time. However, other combinations of phosphorylated and unphosphorylated serines were also present, as well as a completely unphosphorylated peptide, showing that AQP2 when produced in *P. pastoris* is not phosphorylated homogeneously (Table 1). Phosphorylation of Thr[269] could not be verified because of its location at the C terminus where the tryptic digestion results in a fragment that is too low in mass to be detected.

One additional site, Thr[244], was also observed to be phosphorylated by *P. pastoris*. However, this site has not been shown to be phosphorylated *in vivo* (30, 31), and there are no indications that it plays a role in vasopressin-dependent trafficking of AQP2 (4, 32).

Phospho-mimicking mutations and phosphorylation reduce AQP2 thermal stability

The effect of phospho-mimicking mutations on AQP2 overall fold and stability was studied using CD spectroscopy. Far-UV CD spectra between 190 and 260 nm were recorded at 25 °C for wild-type AQP2 that had been dephosphorylated by alkaline phosphatase and AQP2 phospho-mimicking mutants. In addition, we also recorded spectra for AQP2 that had not been treated with alkaline phosphatase and that therefore is phosphorylated as demonstrated by mass spectrometry. All AQP2 variants display very similar spectra with the two local minima at 210 and 222 nm that are characteristic for α-helical proteins (Fig. 3*A*), indicating that the phospho-mimicking mutations do not affect the overall fold of the protein.

The thermal stability of wild-type AQP2 and AQP2 phospho-mimicking mutants was determined by recording CD spectra at different temperatures. By plotting the mean residual ellipticity (MRE) at 222 nm against the temperature and fitting the data to a Boltzmann sigmoidal equation, a melting curve is obtained from which melting temperature (T_M) can be calculated (Fig. 3, *B* and *C*). Dephosphorylated AQP2 exhibited the highest stability with a T_M of 83.5 ± 2.00 closely followed by AQP2-T269E (T_M = 79.2 ± 1.90) (Fig. 3, *B* and *D*). The stability was further reduced for AQP2-S264E and AQP2-S261E, for which T_M was 74.06 ± 1.56 and 73.67 ± 1.58. AQP2 S256E had the lowest stability, with a T_M of 70.07 ± 1.52. AQP2-S256E/T269E displayed a T_M of 73.23 ± 1.95, in between those of the single S256E and T269E mutants.

Similar to the AQP2 phospho-mimicking mutants, untreated AQP2, which is phosphorylated by *P. pastoris* during expression, has a markedly lower stability than dephosphorylated AQP2 (T_M = 74.5 ± 1.65) (Fig. 3, *C* and *D*). Furthermore, the data points for non-treated AQP2 does not fit equally well to the expected Boltzmann sigmoidal equation, in particular in the 20–60 °C range. This may be because this sample represents AQP2 in a variety of phosphorylation states with different

ASBMB

Table 1

Mass spectrometry analysis of AQP2 phosphorylation

All identified peptides assigned to AQP2. Peptide start and end numbering includes the N-terminal His tag. Phosphorylated residues are indicated in bold type. M_r (calculated) indicates the theoretical monoisotopic mass of neutral peptide; ppm, mass accuracy; M, number of missed cleavages.

Start	End	M_r (calculated)	Peptide sequence	Phosphorylation	No. of peptides	Charge	ppm range	M
		Da						
94	121	2821.5490	R.AAFYVAAQLLGAVAGAALLHEITPADIR.G		13	3+, 4+, 5+	1.35–6.41	0
196	205	941.5546	R.SLAPAVVTGK.F		6	2+	2.41–7.23	0
196	236	4470.4184	R.SLAPAVVTGKFDDHWVFWIGPLVGAILGSLLYNYVLFPPAK.S		5	4+	0.35–5.92	1
206	336	3546.8744	K.FDDHWVFWIGPLVGAILGSLLYNYVLFPPAK.S		12	4+, 5+	0.72–3.85	0
242	257	1869.9472	R.LAVLKGLEPDTDWEER.E		4	3+	1.27–6.94	1
247	257	1345.5786	K.GLEPDT²⁴⁴DWEER.E		8	2+	4.28–6.02	0
247	257	1425.5449	K.GLEPDT²⁴⁴**DWEER**.E	T244	5	2+	3.67–7.08	0
247	260	1729.7907	K.GLEPDT²⁴⁴DWEEREVR.R		6	2+, 3+	1.82–5.26	1
247	260	1809.7570	K.GLEPDT²⁴⁴**DWEEREVR**.R	T244	3	2+	3.14–5.28	1
262	275	1632.8696	R.RQS²⁵⁶VELH S²⁶¹PQS²⁶⁴LPR.G		8	2+, 3+, 4+	0.27–4.40	1
262	275	1712.8359	R.RQS²⁵⁶**VELH S²⁶¹PQS²⁶⁴LPR**.G	S256	13	2+, 3+	1.10–5.82	1
262	275	1712.8360	R.RQS²⁵⁶**VELH S²⁶¹PQS²⁶⁴LPR**.G	S261	2	4+	5.11	1
262	275	1792.8023	R.RQS²⁵⁶**VELH S²⁶¹PQS²⁶⁴LPR**.G	S256, S261	7	2+, 4+	2.40–5.10	1
262	275	1872.7686	R.RQS²⁵⁶**VELH S²⁶¹PQS²⁶⁴LPR**.G	S256, S261, S264	4	2+	3.61–4.93	1
263	275	1476.7685	R.QS²⁵⁶VELHS²⁶¹PQS²⁶⁴LPR.G		22	2+, 3+	(−4.52)–6.96	0
263	275	1556.7348	R.QS²⁵⁶**VELHS²⁶¹PQS²⁶⁴LPR**.G	S261	9	2+, 3+	(−3.68)–3.90	0
263	275	1636.7011	R.QS²⁵⁶**VELHS²⁶¹PQS²⁶⁴LPR**.G	S261, S264	2	2+	1.30–1.32	0
263	275	1636.7011	R.QS²⁵⁶**VELHS²⁶¹PQS²⁶⁴LPR**.G	S256, S261	5	2+, 4+	3.04–5.30	0
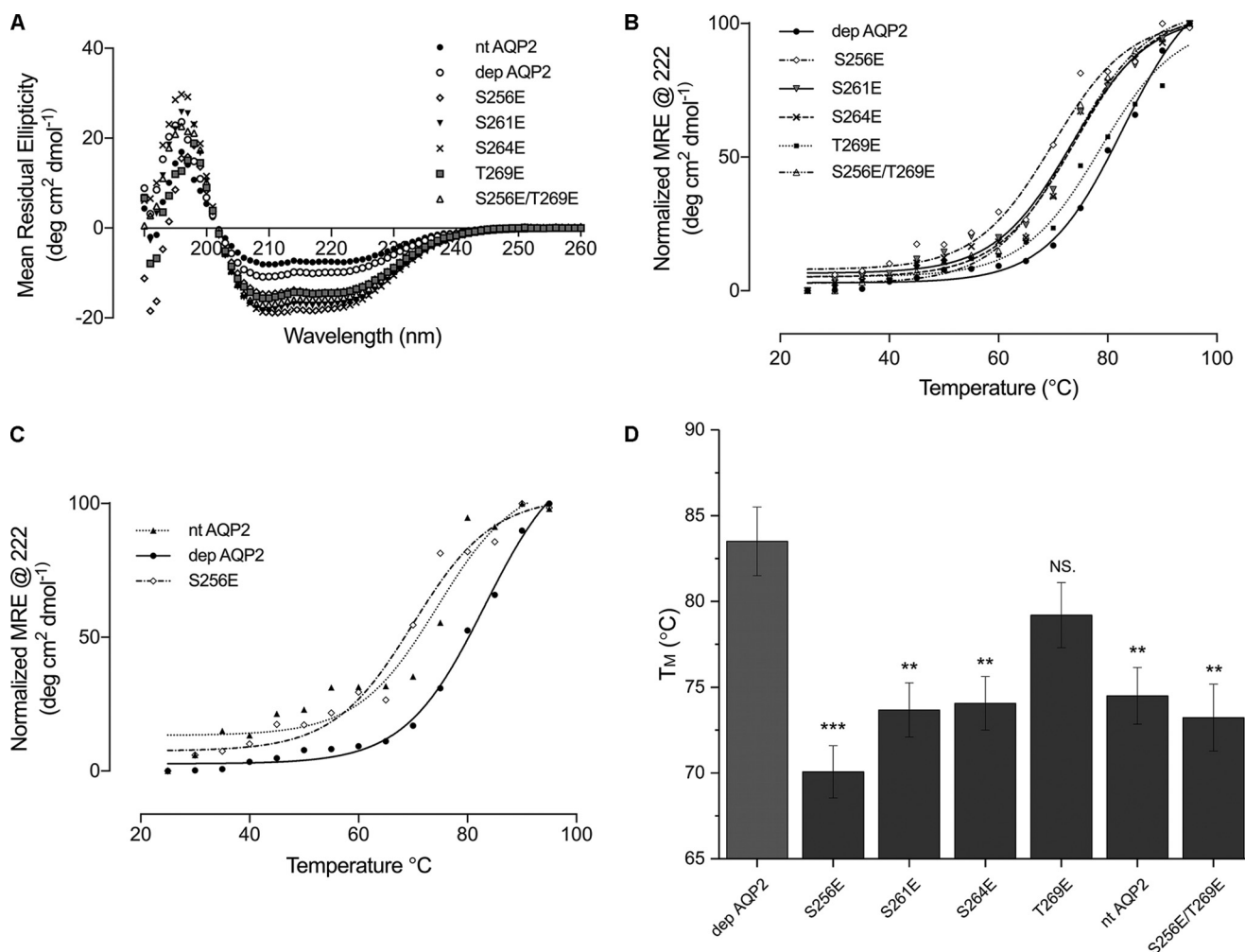
Figure 3. CD spectroscopy and thermal stability of AQP2 and AQP2 mutants. *A*, far-UV CD spectra for non-treated wild-type AQP2 (*nt AQP2*), dephosphorylated wild-type AQP2 (*dep AQP2*), and dephosphorylated AQP2 phosphorylation mutants (S256E, S261E, S264E, T269E, and S256E/T269E). *B*, melting curves for dephosphorylated AQP2 and AQP2 phosphorylation mutants. The curves are obtained by plotting the MRE at 222 nm from CD spectra obtained at different temperatures. *C*, melting curves as in *B* for non-treated wild-type AQP2, dephosphorylated wild-type AQP2, and AQP2-S256E. The melting curve for non-treated AQP2 is more similar to AQP2-S256E than to dephosphorylated AQP2. *D*, bar chart displaying melting temperatures for the different AQP2 constructs. All phosphorylation mutants have a significantly lower T_M than dephosphorylated AQP2 (*** indicates $p < 0.001$, and ** indicates $p < 0.01$; *NS* indicates not significant).

melting behaviors. A deviation from sigmoidal behavior in a similar temperature range is also seen for dephosphorylated AQP2 and the phospho-mimicking mutants (Fig. 3*C* and supplemental Fig. S2), although to a smaller extent. This could be interpreted as a minor transition representing an unfolding event prior to the major transition, possibly of flexible regions such as the termini. In this respect, it is interesting to note that this minor transition varies somewhat in extent and temperature range between the different phosphorylation mutants (supplemental Fig. S2), suggesting phosphorylation-induced differences in the structure of the C terminus.

Phospho-mimicking mutations and C-terminal truncation affects the interaction between AQP2 and LIP5

The interaction between AQP2 and LIP5 and its dependence on phosphorylation and C-terminal truncation was initially explored using the far-Western blot technique (33). To ensure a phosphorylation-free background, all AQP2 constructs were dephosphorylated after purification, with the exception of AQP2-ΔP242 in which phosphorylation sites are removed by truncation. Incubation of purified AQP2 with alkaline phosphatase for 2 h resulted in complete dephosphorylation, as illustrated in Fig. 2*A* (*lane 2*). A Western blot stained with antibodies against the His tag confirms that AQP2 is present in the dephosphorylated sample (Fig. 2*B*, *lanes 2–4*). The dephosphorylated proteins were additionally purified using size exclusion chromatography prior to further studies.

Equal amounts of purified wild-type AQP2, AQP2 phospho-mimicking mutants (S256E, S261E, S264E, T269E, and S256E/T269E), AQP2-ΔP242, and human AQP4 (negative control) were run on an SDS-PAGE gel, transferred to a nitrocellulose membrane, denatured with guanidine HCl, and re-natured, thereby regaining their native secondary and tertiary structure. After blocking and incubation with LIP5 overnight, the AQP2-LIP5 interaction was probed using an antibody directed against LIP5 (20).

As seen in Fig. 4*A*, LIP5 interacts with wild-type AQP2, whereas no interaction was observed with AQP4. Furthermore, although all phospho-mimicking mutants show a positive signal for LIP5 interaction, there is a distinct variation in the signal strength. Staining with antibody directed against the His tag (Fig. 4*B*) and Ponceau reagent (Fig. 4*C*) showed that protein equivalents had been loaded, illustrating that the observed signal strength variation was not due to differences in protein amounts. Quantification of the signal relative to wild-type AQP2 (Fig. 4*D*) revealed that AQP2-S256E, AQP2-S261E, and AQP2-S264E show reduced binding, equivalent to 55 ± 1.2, 63 ± 3.5, and 59 ± 2.5% of the wild-type signal, respectively. The signal for AQP2-T269E is more similar to wild-type AQP2, the relative intensity is 80 ± 12%. The double AQP2-S256E/T269E mutant behaved similarly as the single mutant AQP2–256E with relative intensity signal of 54 ± 6.4%. Interestingly, AQP2 lacking the distal part of the C terminus containing the phosphorylation sites (AQP2-ΔP242) yielded in the lowest interaction signal corresponding to 22 ± 5.9% of wild-type AQP2. This suggests that the distal C terminus and its phosphorylation status modulate the interaction between AQP2 and LIP5.

AQP2-S256E, S261E, T269E, S256E/T269E, and ΔP242 have significantly lower affinity to LIP5 than wild-type AQP2

The effect of phosphorylation on the AQP2-LIP5 interaction was further studied by determining complex affinities using MST, a method that detects complex formation from a change of movement in a thermal gradient. As for the far-Western blot analysis, wild-type AQP2 and AQP2 phospho-mimicking mutants were dephosphorylated prior to the experiment. For each protein, a 1.5-fold (wild-type AQP2 and AQP2 phospho-mimicking mutants) or 2-fold dilution series (AQP2-ΔP242 and AQP4) was made, resulting in 16 different samples. Each sample was mixed 1:1 with a constant concentration of LIP5, fluorescently labeled with the amine-reactive dye (NT-647-NHS), and MST traces were recorded (supplemental Fig. S3). This resulted in a binding curve from which the dissociation constant K_d could be determined (Fig. 5 and supplemental Fig. S4).
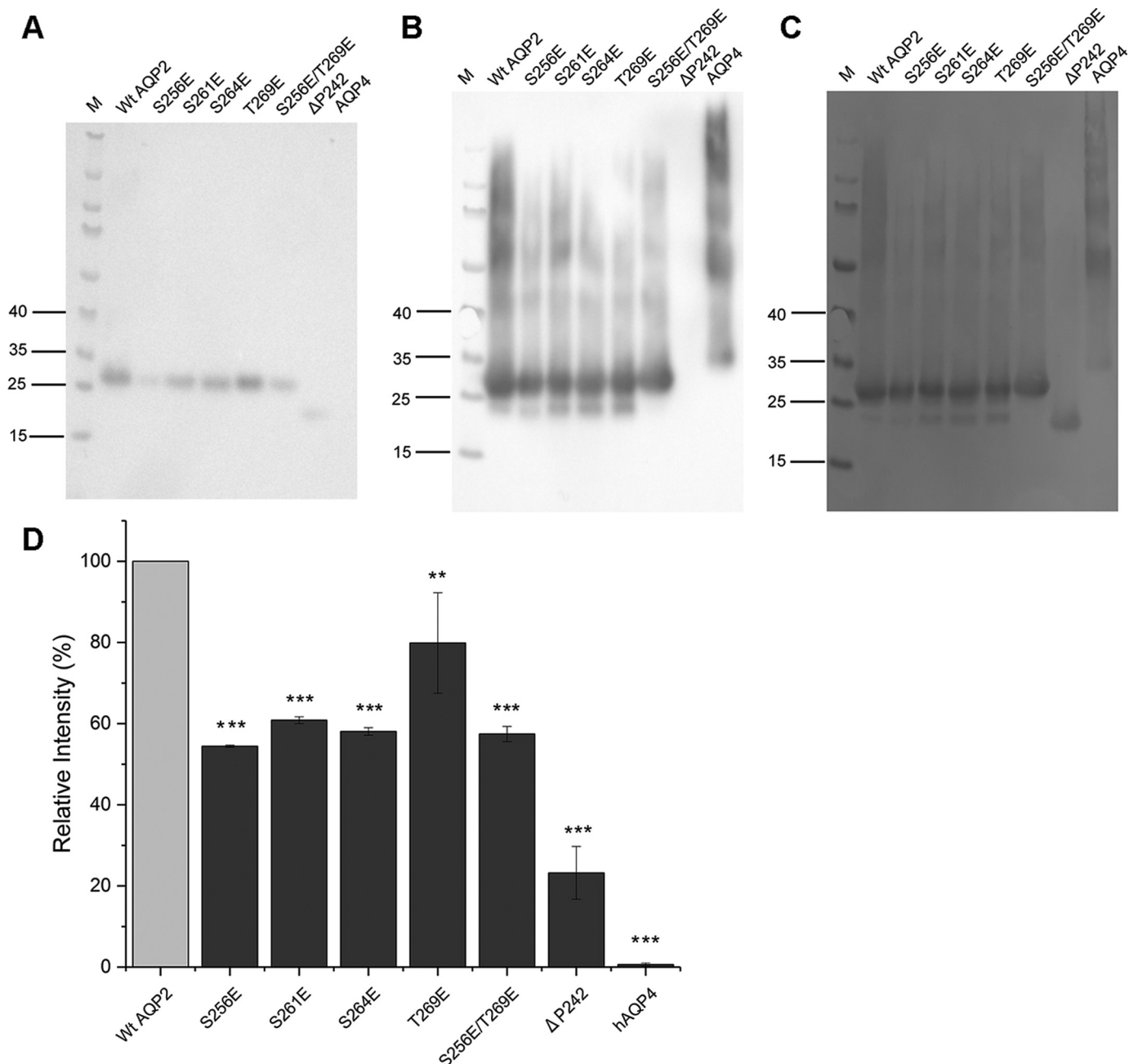
Non-phosphorylated wild-type AQP2 binds LIP5 with a K_d of 191 ± 43.2 nM (Fig. 5, *A* and *D*). For AQP4 there is a variation in fluorescence signal (ΔF_{norm}); however, the data points are scattered, and saturation is never reached. Hence, the data cannot be fitted to a binding curve, wherefore we conclude that the data do not describe a concentration-dependent interaction between AQP4 and LIP5. This is further supported by the far-Western blot in which LIP5 did not bind to AQP4 (Fig. 4).

As seen in Fig. 5*B*, removing the distal part of the C terminus significantly reduces the affinity: the K_d for the interaction between AQP2-ΔP242 and LIP5 is almost 20-fold higher than for wild-type AQP2 ($K_d = 3.63 ± 0.44 \mu M$) (Fig. 5*D*). Four of five AQP2 phospho-mimicking mutants bind LIP5 with lower affinity than wild-type AQP2 (Fig. 5, *C* and *D*). The lowest affinity is seen for AQP2-S256E ($K_d = 1.00 ± 0.25 \mu M$), the protein that mimics AQP2 phosphorylated at the most crucial site for apical membrane targeting. The affinity is also significantly lower for AQP2-S261E ($K_d = 745 ± 141$ nM), AQP2-T269E ($K_d = 721 ± 55.0$ nM), and AQP2-S256E/T269E ($652.7 ± 62.2$ nM), whereas AQP2 S264E binds LIP5 with almost the same affinity as non-phosphorylated wild type ($K_d = 278 ± 49.1$ nM).

Plotting log K_d against $1/T_M$ for wild-type AQP2 and phospho-mimicking AQP2 mutants reveals a linear relationship (Fig. 6). This suggests an empirical correlation between LIP5 affinity and AQP2 stability where AQP2-S256E, the mutant with the lowest LIP5 affinity, also has the lowest thermal stability. The correlation seems to be weaker for the more distal mutation sites S264E and T269E, whereas the double S256E/T269E mutant behaves according to linearity.

The distal AQP2 C terminus does not interact with the AQP2 LIP5 binding site or with LIP5

One possible explanation for the lower affinity between LIP5 and AQP2 phospho-mimicking mutants could be that the phosphorylated distal AQP2 C terminus interacts with the LIP5 binding site within the proximal AQP2 C terminus (Fig. 1), thereby preventing the interaction. To investigate this scenario, we used MST to study whether peptides corresponding to the distal AQP2 C terminus (residues 244–271) phosphorylated at Ser[256], Ser[261], Ser[264], and Thr[269], respectively, are able to inter-

ASBMB

Figure 4. Far-Western blot analysis of the interaction between AQP2 and LIP5. Equal amounts of dephosphorylated wild-type AQP2, AQP2 mutants, and AQP4 were transferred to a nitrocellulose membrane and incubated with purified LIP5. The interaction was detected using an antibody directed against LIP5. *A*, typical far-Western blot showing that wild-type AQP2, but not AQP4, interacts with LIP5. AQP2-S256E, S261E, S264E, T269E, S256E/T269E, and ΔP242 all interact with LIP5 but show significant variation in signal strength. *B* and *C*, staining the membrane with antibodies against the His tag (*B*) and Ponceau reagent (*C*) confirmed that protein equivalents had been loaded in each lane. AQP2-ΔP242 does not contain a His tag and is consequently not stained with anti-His antibodies (*B*). Marker protein masses are indicated in kDa. *D*, relative intensities of far Western blot signal for AQP2 mutant constructs and AQP4 compared with wild-type AQP2 (set as 100%). The values were calculated from three independent blots. The AQP2 variants S256E, S261E, S264E, and S256E/T269E show significantly less binding than wild-type AQP2 ($p < 0.001$, indicated by ***) but were not significantly different from each other. The binding was further reduced for ΔP242 ($p < 0.001$), whereas the signal intensity of AQP2 T269E was more similar to wild-type ($p < 0.01$, indicated by **). AQP4 did not interact with LIP5 ($p < 0.001$).

act with AQP2 itself. For this experiment, a 1.5-fold dilution series was made of each peptide, resulting in 16 samples that were mixed 1:1 with wild-type AQP2 that had been fluorescently labeled with the cysteine-reactive dye Alexa-488, and MST traces were recorded (supplemental Fig. S5A). The final concentration of AQP2 in all samples was 500 nM. As shown in supplemental Fig. S6, no interaction with full-length AQP2 could be observed for any of the phosphorylated peptides.

Next, we used MST to study whether the unphosphorylated or phosphorylated distal C terminus could interact with LIP5 on its own. Similar as above, a 2-fold dilution series of the phosphorylated AQP2 C-terminal peptides, as well as the corresponding unphosphorylated peptide, was mixed 1:1 with fluorescently labeled LIP5 at a final concentration of 45 nM, and MST traces were recorded (supplemental Fig. S5B). Neither the unphosphorylated nor the phosphorylated distal C terminus
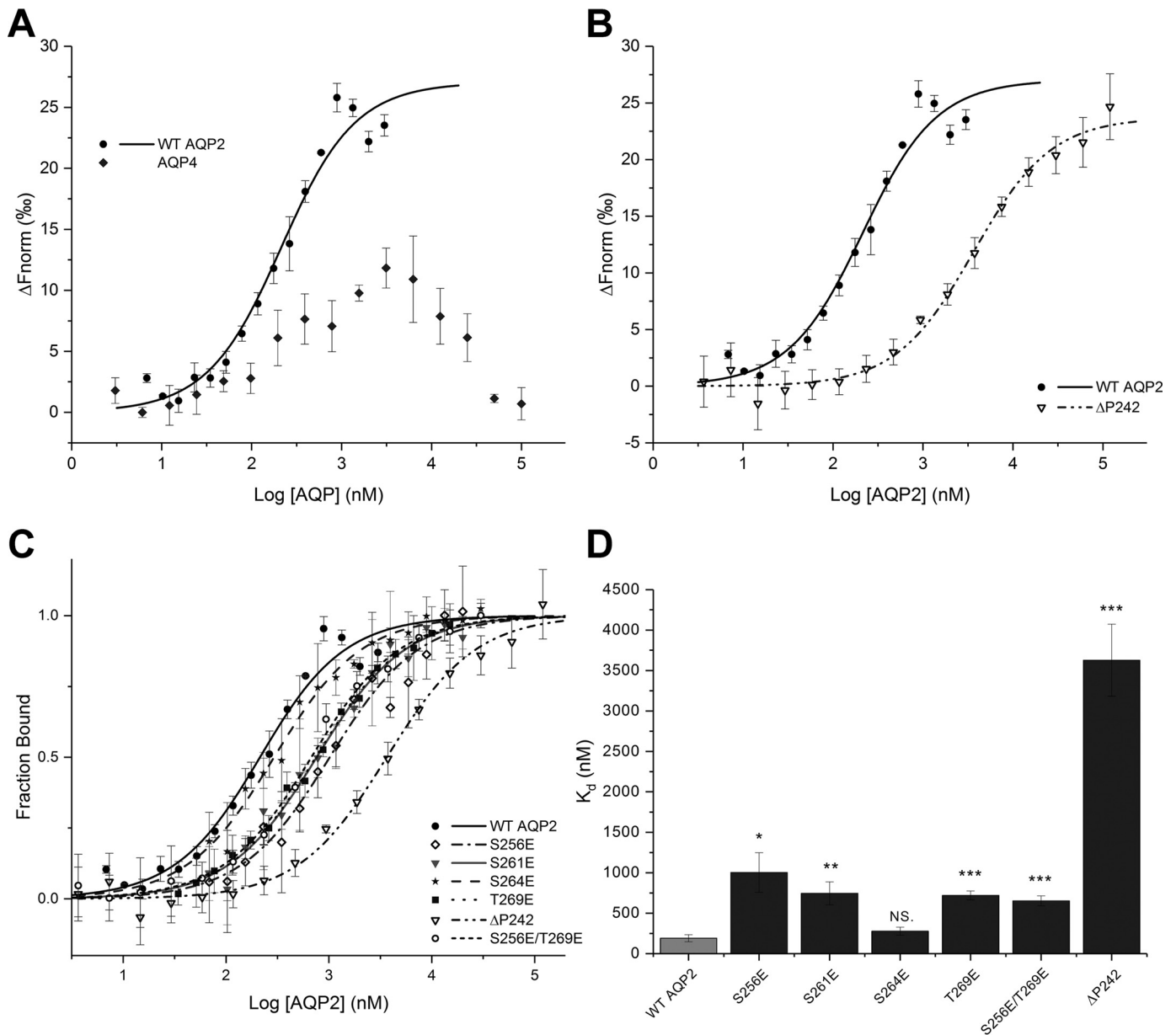
Figure 5. Phosphorylation modulates the affinity between AQP2 and LIP5. The interaction between LIP5 and AQP2 was measured with MST, and the data were fitted according to a one-to-one binding model. *A*, dephosphorylated WT AQP2 interacts with LIP5 ($K_d = 191 \pm 43.2$ nM). The data for AQP4 (negative control) had a low amplitude, could not be fitted to the equation, and did not reach saturation; therefore binding was interpreted as non-significant. *B*, C-terminal truncation of AQP2 (ΔP242) reduces the affinity 20-fold ($K_d = 3.63 \pm 0.44$ μM). *C*, comparison of MST curves for WT AQP2 and phospho-mimicking mutants. There is a significant difference between WT and S256E ($K_d = 1.00 \pm 0.25$ μM), S261E ($K_d = 745 \pm 141$ nM), T269E ($K_d = 721 \pm 55.0$ nM), and S256E/T269E (652.7 ± 62.2 nM) (*, $p < 0.05$; **, $p < 0.01$; ***, $p < 0.001$). There is no significant difference between WT and S264E ($K_d = 278 \pm 49.1$ nM). *D*, bar chart summarizing K_d values determined in *A–C*.

interacted with LIP5 (supplemental Fig. S7). Taken together, these experiments show that AQP2 phosphorylation does not reduce LIP5 affinity by blocking the binding site on either AQP2 or LIP5 and that the distal C terminus does not bind LIP5 independently.

Discussion

Protein-protein interactions lie at the heart of intracellular membrane protein trafficking, governing recruitment of membrane protein cargo to specific transport vesicles and directing these vesicles to the correct membrane domain at the correct time (14, 15). Because vasopressin-mediated phosphorylation

is known to regulate AQP2 endo- and exocytosis (2–4, 7–10), this likely relies on changed affinities between phosphorylated AQP2 and members of the membrane protein sorting and trafficking machinery. Indeed, several proteins have been shown to preferentially interact with unphosphorylated or phosphorylated AQP2 (11, 22). However, most of these studies are based on co-immunoprecipitation, yeast two-hybrid assays, or mass spectrometry and are therefore unlikely to catch the dynamic regulation that more subtle differences in affinities are able to confer.

The interaction between AQP2 and LIP5 was first demonstrated using a yeast two-hybrid assay in which the C-terminal tail of AQP2 had been fused to LexA (20). Using a colony-based
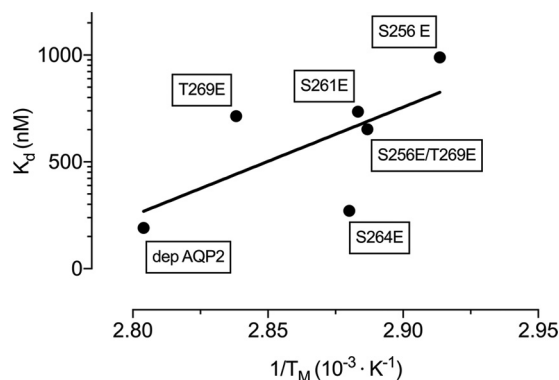
Figure 6. LIP5 affinity correlates with AQP2 stability. Plotting the dissociation constant (log K_d) for the interaction between AQP2 variants and LIP5 against the inverted AQP2 melting temperature ($1/T_M$) reveals a linear relationship ($R^2 = 0.4369$). The correlation is weaker for the more distal mutation S264E and T269E, whereas the double S256E/T269E mutant fits well to the linearity.

β-galactosidase assay, it was concluded that AQP2 binds LIP5 via residues Leu[230]–Asp[243], because truncation beyond Leu[230] abolished binding, whereas truncation beyond Asp[243] did not. Sequence analysis reveals that this region contains a motif, LSERLAVLK, perfectly matching the MIM1 (MIT-interacting motif 1) core sequence LXXRϕ$L$$XX$L(K/R) (where ϕ is any hydrophobic residue, most often Leu) (34). A MIM1 motif has previously been shown to mediate interaction between a component of the ESCRT-III complex (CHMP1B) and the LIP5 N-terminal MIT domain (24). In the crystal structure of human AQP2, the same motif was involved in protein-protein interactions between symmetry-related AQP2 molecules in the crystal packing (26), possibly mimicking how AQP2 interacts with LIP5. Here, we show that AQP2-ΔP242 binds LIP5 directly, thereby supporting earlier data showing that the distal part of the C terminus is not essential for the ability of AQP2 to interact with LIP5 (20). However, truncation beyond Pro[242] significantly reduces the affinity, suggesting that the distal C terminus somehow affects LIP5 binding. Whether this involves direct binding between the distal C terminus and LIP5 remains to be elucidated. Our experiment showing that a peptide corresponding to the distal AQP2 C terminus does not bind LIP5 on its own (supplemental Fig. S7) suggests that if they do interact, this is dependent on the interaction between LIP5 and the MIM1 motif within the proximal AQP2 C terminus. Alternatively the distal C terminus may not be directly involved in LIP5 binding; instead its presence may affect the overall structure of the C terminus and/or its position relative to the tetramer.
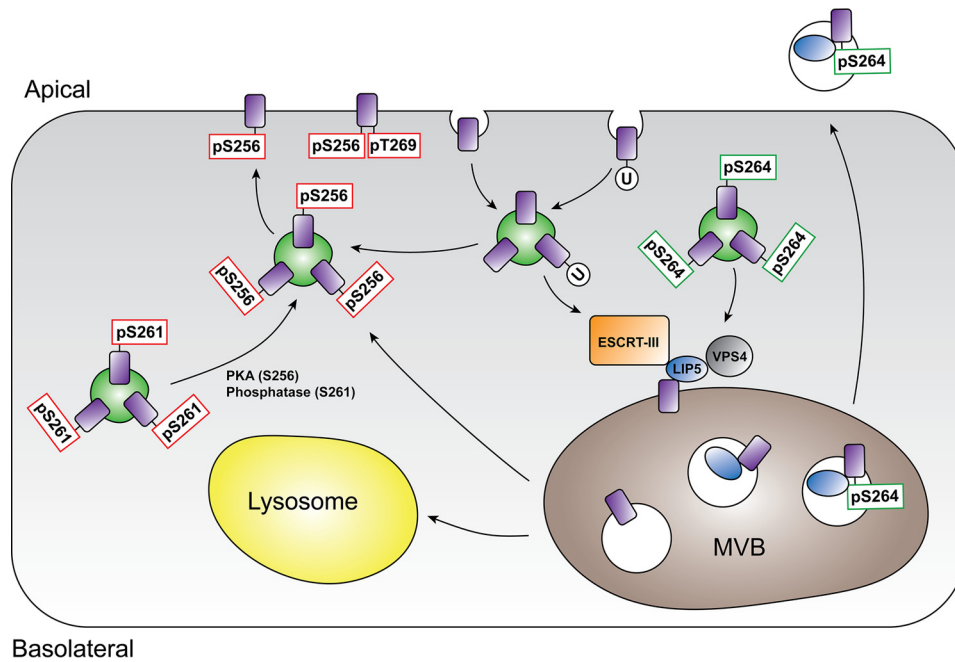
Although the details of how the distal AQP2 C terminus plays a role in LIP5 binding is not known, we show that introducing phospho-mimicking mutations at four known phosphorylation sites within this region modulates the interaction between AQP2 and LIP5. Our far-Western blot and MST analysis of interaction between AQP2 and LIP5 are in good agreement, with two exceptions: AQP2-S264E and AQP2-T269E. AQP2-S264E displays a low interaction signal in the far-Western blot (Fig. 4), whereas the K_d determined by MST is similar to wild-type AQP2 (Fig. 5, *C* and *D*). In the case of AQP2 T269E, the situation is opposite; K_d is higher than for wild-type AQP2, suggesting lower affinity, whereas the far-Western blot signal is not significantly different. These discrepancies may arise from

method differences, such as the fact that in far-Western blot, the proteins are immobilized, whereas in MST they are in free solution. The crystal structure of AQP2 showed that the C terminus is capable of adopting several different positions relative to the tetramer, highlighting a flexibility that had not previously been observed in eukaryotic AQPs (26). If the C-terminal position plays a role in determining the affinity between AQP2 and LIP5, this is much more likely to be picked up in MST than in far-Western blot and could explain the differences observed here.

Our data suggest that phosphorylation of AQP2 serves as an allosteric trigger, affecting the interaction with LIP5 by inducing conformational changes within the C terminus or modulating binding to a secondary binding site within LIP5. Phosphorylation-induced structural changes of the C terminus could explain the correlation between AQP2 thermal stability and LIP5 affinity (Fig. 6), assuming that CD detects these changes. Previous work by Zwang *et al.* (22) supports this, showing that an AQP2 C-terminal peptide phosphorylated on Ser[256] is less α-helical than its non-phosphorylated counterpart, whereas an AQP2 C-terminal peptide phosphorylated on Ser[261] had an α-helical content somewhere in between. This fits with our results: AQP2-S256E has the lowest affinity and stability, whereas AQP2-S261E has the second to lowest. The correlation between stability and affinity seems to be weaker for the more distal mutation sites S264E and T269E. However, although the single T269E mutant deviates from linearity, the double S256E/T269E mutant does not. Because phosphorylation of S256E precedes phosphorylation of T269E, this represents an AQP2 phosphorylation state that is more likely to exist in the cell. Thus, the only physiologically relevant phospho-mimicking mutant that does not fit into the linear relationship between affinity and stability is AQP2-S264E. It is interesting to note that for this mutant (as well as for AQP2-T269E), the far-Western blot and MST showed different results in binding activity when compared with wild-type AQP2. We speculate that this may reflect differences in the type of structural perturbations caused by the phospho-mimicking mutations. For example one mutation may cause a loss of helical structure of the C terminus, as suggested above for S256E and S261E, whereas another mainly affects its position relative to the tetramer. Although both structural perturbations might reduce LIP5 affinity to a similar extent, their differences in overall structure could be reflected in thermal stability.

Based on what is known about the roles of AQP2 phosphorylation sites in the cell and the established role of LIP5 in targeting AQP2 to MVBs, we propose the following hypothesis for how phosphorylation-regulated interactions with LIP5 affect AQP2 sorting *in vivo* (Fig. 7). In unstimulated conditions, AQP2 is phosphorylated at Ser[261] and kept in storage vesicles. To maintain this intracellular pool of AQP2, the affinity to LIP5 is low. Vasopressin-mediated phosphorylation at Ser[256] further reduces the affinity to LIP5, ensuring that AQP2 is efficiently translocated to the apical membrane. Once at the apical membrane, additional phosphorylation of Thr[269] reduces AQP2 internalization, increasing the AQP2 apical membrane amount. Phosphorylation of this residue also reduces AQP2 affinity to LIP5. The highest LIP5 affinity is seen for non-phosphorylated AQP2, suggesting that this form of the protein

Figure 7. Model for the role of AQP2 phosphorylation in regulating LIP5-mediated targeting to MVBs. *Red* and *green boxes* indicate phosphorylation sites with decreased and increased affinity to LIP5, respectively. During unstimulated conditions, AQP2 resides in storage vesicles and is mainly phosphorylated on Ser[261]. Dephosphorylation of Ser[261] and phosphorylation of Ser[256] trigger targeting of AQP2 to the apical membrane, whereas additional phosphorylation at Thr[269] further increases the AQP2 apical membrane residence time. Phosphorylation at these three sites reduces LIP5 affinity. Dephosphorylation, as well as ubiquitination of AQP2, in the apical membrane induces endocytosis. Dephosphorylated AQP2 has the highest affinity for LIP5, stimulating its sorting into the inner vesicles of MVBs by coordinating the actions of ESCRT-III complex and VPS4. AQP2 phosphorylated at Ser[264] also has higher affinity for LIP5 and may be involved in sorting AQP2 into MVBs for secretion in exosomes.

is targeted to MVBs for subsequent degradation in the lysosome. Interestingly, our data suggest that the affinity between LIP5 and AQP2 phosphorylated at Ser[264] is almost as high as seen for non-phosphorylated AQP2. Ser[264] phosphorylation is believed to be involved in intracellular sorting of AQP2 and has been suggested to play a role in AQP2 excretion via exosomes (7). Because exosomes originate from the internal vesicles of MVBs (6), our data may indicate that Ser[264] phosphorylation of AQP2 increases the targeting of AQP2 to exosomes by increasing its affinity for LIP5.

In summary, the results presented here show, for the first time, that AQP2 phosphorylation regulates its interaction with the lysosomal sorting protein LIP5. Importantly, we use purified full-length proteins to quantitatively investigate direct interactions, thereby allowing us to describe a highly dynamic process in which the distal C terminus allosterically regulates the interaction with LIP5 in a phosphorylation-dependent manner. Further investigations of how post-translational modifications affect the interaction between AQP2 and LIP5, as well as other proteins, will give detailed knowledge of how protein-protein interactions govern AQP2 sorting and provide a platform by which structural studies of AQP2-interaction protein complexes can be explored.

Experimental procedures

Cloning and expression of LIP5

Full-length mouse LIP5 was amplified by PCR from pCDNA3 encoding a previously described LIP5 construct (20) using 5-GATTTGTTATTCCATATGGCCGCGCTGGCCC-CTCTGCCG-3′ (sense) and 5′-CTTGGATCCTTAATGA-TGATGATGATGATGACCCTGAAAATACAAGTTTTCGG-TAGTTGGGATATCGTAATCCTCCCTGCCTGTGGT-CAGCAG-3′ (antisense) as forward and reverse primers, respectively. NdeI and BamHI restriction sites used for cloning into the pET3a vector (Novagene) are underlined. The encoded LIP5 product contains a C-terminal His$_6$ tag preceded by a tobacco etch virus (TEV) protease cleavage site (ENLYFQG). A seven-amino acid spacer (DYDIPTT) is included between the last residue of LIP5 and the TEV site to ensure efficient proteolytic cleavage.

LIP5 was expressed in BL21* (DE3) *Escherichia coli* (Invitrogen). The cells were grown in LB media containing 50 μg/ml ampicillin. On reaching mid-log phase at an approximate A_{600} of 0.8, the cells were induced with 0.5 mM isopropyl β-D-1-thiogalactopyranoside for an additional 3.5–4 h. The cells were then harvested at 6000 × *g* for 15 min.

Purification of LIP5

4 g of cells were resuspended in 50 ml of lysis buffer (20 mM Tris, pH 8, 250 mM NaCl, 5% glycerol, 10 mM imidazole) supplemented with one cOmplete™ EDTA-free protease inhibitor mixture tablet (Roche). The cells were lysed using 10 × 1-min sonication with 1-min intervals while being kept on ice. Unbroken material was pelleted at 18,000 × *g* at 4 °C for 30 min, and the cell lysate was filtered before loading onto a 5-ml Ni^{2+}-nitrilotriacetic acid-affinity column equilibrated with lysis buffer. After two wash steps with lysis buffer containing 30 and 100 mM imidazole, respectively, LIP5 was eluted with the same buffer containing 250 mM imidazole. The samples were analyzed on SDS-PAGE, and the fractions corresponding to LIP5

were pooled and concentrated using a 10-kDa molecular mass cutoff Vivaspin concentration tube (GE Healthcare). LIP5 was further purified from the concentrated sample by size exclusion chromatography, using a Superdex 200 10/300 GL column (GE Healthcare) and LIP5 buffer (20 mM Tris, pH 8, 150 mM NaCl, 1 mM DTT). Fractions containing LIP5 were analyzed for purity using SDS-PAGE, pooled, and concentrated as above. The sample was used directly or supplemented with glycerol (10% final concentration), flash-frozen in liquid nitrogen, and stored at −80 °C.

Cloning, expression, and purification of AQP2, AQP2 mutants, and AQP4

Full-length human AQP2, AQP2-ΔP242, and human AQP4 were expressed in *P. pastoris* as described (26). Both AQP2 constructs contain a N-terminal His$_8$ tag, whereas AQP4 contains a C-terminal His$_8$ tag. AQP2-ΔP242 also contains a TEV site immediately following the His tag, whereas this is not present in full-length AQP2. AQP2 phosphorylation mutants (S256E, S261E, S264E, and T269E) were generated using a standard PCR mutagenesis protocol (QuikChange; Agilent). The S256E/T269E mutant was created using a megaprimer mutagenesis protocol as described in Tseng *et al.* (35). Briefly, the cells were grown in a 3-liter fermentor (Belach, Bioteknik), and protein expression was induced using methanol for 24–36 h. Routinely, 50–100 g of cells were lysed by 12 × 30-s bead beating cycles with 30 s of waiting in between each cycle. The cell lysate was centrifuged at 10,000 × *g* for 40 min to remove unbroken cells and cell debris, after which membranes were isolated from the supernatant by ultracentrifugation at 100,000 × *g* for 1 h. The membranes were homogenized and washed twice, first using wash buffer (5 mM Tris-HCl, pH 9.5, 4 M urea, 2 mM EDTA) followed by membrane buffer (20 mM Tris-HCl, pH 8, 20 mM NaCl, 10% glycerol) supplemented with 1 mM PMSF and 2 mM EDTA. The membranes were finally resuspended in membrane buffer to a final concentration of 0.5 g/ml and stored at −80 °C until further use.

The membranes were diluted 1:1 with 25 ml solubilization buffer (20 mM Tris-HCl, pH 8, 300 mM NaCl, 4% octyl glucoside neopentyl glycol (OGNPG; Anatrace) supplemented with one cOmplete™ EDTA-free protease inhibitor mixture tablet (Roche) with continuous stirring for 1 h at 4 °C. Final solubilization volume and detergent concentration was 50 ml and 2%, respectively. Unsolubilized material was pelleted at 100,000 × *g*. The supernatant was supplemented with imidazole to a final concentration of 10 mM and loaded on a nickel-affinity column (HisTrap, GE Healthcare) equilibrated with AQP2 buffer (20 mM Tris-HCl, pH 8, 300 mM NaCl, 10 mM imidazole, 0.2% OGNPG). After washing with the same buffer containing 75 mM imidazole, AQP2 was eluted using 300 mM imidazole. Fractions were analyzed using SDS-PAGE, pooled, and concentrated using a Vivaspin concentrator with 50-kDa cut-off. The concentrated sample was loaded on a Superdex 200 10/300 GL (GE Healthcare) equilibrated with the AQP2 buffer. After SDS-PAGE analysis, relevant fractions were pooled and concentrated as above.

For AQP2-ΔP242 the His tag was removed as an additional purification step prior to gel filtration. Following elution from the nickel-affinity column, the imidazole was removed by desalting to AQP2 buffer on a PD-10 column (GE Healthcare). The protein was incubated with TEV protease (35) in a 1:2 AQP2:TEV protease ratio. The sample was supplemented with 0.5 μM TCEP and incubated on a rotating table at 4 °C, overnight. Precipitate was removed with a 0.45-μm syringe filter, and the sample was loaded on a nickel-affinity column equilibrated with AQP2 buffer supplemented with 20 mM imidazole. The flow-through was collected, concentrated, and further treated as the other AQP2 constructs.

AQP4 was purified similarly to AQP2 but with the following alterations: The membranes were solubilized in 20 mM Tris-HCl, pH 8, 300 mM NaCl, 10% glycerol, 4% β-octyl glucoside supplemented with one cOmplete protease inhibitor tablet for 2.5 h at 4 °C. Nickel-affinity chromatography was performed in 20 mM Tris-HCl, pH 8, 300 mM NaCl, 10% glycerol, 1% β-octyl glucoside. The column was washed with the same buffer supplemented with 75 mM imidazole and protein eluted using 300 mM imidazole. AQP4 was further purified by SEC using an Enrich 650 10 × 300 (Bio-Rad) in 20 mM Tris-HCl, pH 8, 300 mM NaCl, 0.2% OGNPG.

Dephosphorylation

Purified AQP2 was treated with alkaline phosphatase in 5 mM Tris-HCl, pH 7.9, 10 mM NaCl, 1 mM MgCl$_2$, and 0.1 mM DTT and incubated at 30 °C for different time interval of 2, 4, and 20 h. For Far Western blot and MST experiments, wild-type AQP2 and AQP2 phospho-mimicking mutants were treated with alkaline phosphatase for 2 h and subsequently purified using size-exclusion chromatography as described above.

Phosphorylation analysis

Untreated and dephosphorylated AQP2 were probed for phosphorylation using a biotinylated phosphate binding tag (Phos-tag™ BTL-111; Wako Pure Chemical Industries, Ltd). The experimental procedure implemented is described in detail by Kinoshita *et al.* (36) with slight modification as mentioned in Ampah-Korsah *et al.* (28). Briefly, equal amounts of untreated and treated AQP2 were run on an SDS-PAGE gel, after which the proteins were transferred onto a PVDF membrane for 1 h at 100 V. The membrane was blocked with 10% (w/v) BSA in TBS-T for 6 h followed by overnight incubation with a complex between Phos-tag BTL-111 and streptavidin-conjugated horseradish peroxidase (HRP-SA) to detect protein phosphorylation. The Phos-tag BTL-111/HRP-SA complex was prepared by mixing 5 μl of 10 mM aqueous solution of Phos-tag BTL-111, 20 μl of 10 mM aqueous solution of Zn(NO$_3$)$_2$, 1 μl of HRP-SA (GE Healthcare Biosciences), and 469 μl of TBS-T (10 mM Tris-HCl, pH 7.5, 100 mM NaCl, 0.1% Tween 20) followed by incubation in the dark for 1 h at room temperature. The mixture was then transferred into a 30 K Nanosep filtration column (Pall Corporation) and spun for 6 min at 14,000 × *g* to remove excess Phos-tag BTL-111. The remaining solution (>10 μl) was diluted with 25 ml of TBS-T solution containing 1% (w/v) BSA and 1 M sodium acetate and used for incubation as described above. The membrane was washed twice, 5 min/wash with TBST containing 1% (w/v) BSA and 1 M sodium acetate. The

blot was developed using ECl chemiluminescence (GE Healthcare).

For the control blot stained with an antibody against the His tag, equal amounts of untreated and treated AQP2 were run on an SDS-PAGE gel, after which the proteins were transferred onto a PVDF membrane for 1 h at 100 V. The membrane was treated in a similar way as for the phosphorylation analysis blot, where the membrane was blocked with 10% (w/v) BSA in TBS-T for 6 h followed by overnight incubation with anti-His antibody (His$_6$ monoclonal antibody, 631212 (albumin free), Clontech), diluted 1:5000 in 5% milk in TBS-T for 1 h. After washing three times for 5 min each, the membrane was incubated with a secondary antibody (anti-mouse IgG, 374-1806; Kirkegaard and Perry Laboratories) diluted 1:5000 in 5% milk in TBS-T for 1 h. Finally, the membrane was washed three times for 5 min in TBS-T and developed using ECL chemiluminescence (GE Healthcare).

Mass spectrometry sample preparation and data collection

Purified full-length AQP2 was first treated with iodoacetamide to alkylate cysteines (19, 37). Afterward the protein sample was denatured using a solution containing 6 M urea and sequentially digested with LysC and trypsin or not denatured and digested with trypsin only. The resulting peptides were purified using C18 microcolumn and separated using online reversed phase nano-LC system. Mass spectrometry analysis of the protein was done using LTQ Orbitrap Velos Pro mass spectrometer (Thermo Fisher Scientific), coupled with a nanoEasy spray ion source (Proxeon Biosystems).

Mass spectrometry data analysis

Peak picking was performed by Mascot Distiller version 2.6.1.0 using default settings. A peptide mass fingerprint search in Mascot Daemon version 2.5.1 using our own database with AQP2 sequence resulted in 38% protein sequence coverage ($p < 0.05$). The peptide mass tolerance was $\pm$ 10 ppm, and a maximum of one missed cleavage was allowed. Phosphorylation on serine or threonine was added to the search as variable modification. 40 non-duplicate peptides were identified and confirmed by MS/MS. For MS/MS search, the mass tolerance was set to $\pm$ 0.5 Da.

CD spectroscopy and data analysis

Briefly, purified non-treated and dephosphorylated wild-type AQP2 and AQP2 phospho-mimicking mutants were diluted with 10 mM potassium phosphate, pH 7.5, 100 mM NaCl, 0.2% OGNPG, 5% glycerol to a final concentration of 0.2 mg/ml. The protein solution was added to a quartz cuvette with 0.1-cm path length, and the far UV CD spectra between 260 and 190 nm were obtained in Jasco J-720 spectrometer (Jasco, Tokyo, Japan) at 25–95 °C with a scanning speed of 20 nm/min. The sample temperature was controlled by a built-in Peltier controller. An average of three scans were recorded with a data pitch of 1 nm and a response time 8 s. The spectra were baseline corrected using the similar settings.

MRE ($[\theta] \times 10^{-3}$ deg cm^2 dmol^{-1}) was calculated using the following equation,

$$MRE = M \times \theta/(10 \times l \times c \times n) \qquad \text{(Eq. 1)}$$

where M is the molar mass of the protein (29,000 g/mol), θ is the measured ellipticity in millidegrees, l is the cell path length (0.1 cm), c is the concentration in g/liter (0.2 g/liter), and n is the number of residues ($n = 271$).

The MRE at 222 nm was plotted against temperature. For curve fitting, the following Boltzmann sigmoidal equation was used,

$$Y_{obs} = \text{bottom} + ((\text{top} - \text{bottom}))/1 + \exp(TM - T)/\text{slope}$$

$$\text{(Eq. 2)}$$

where Y_{obs} is the MRE, and T_M is the temperature at which MRE is halfway between native and denatured state. Global analysis of thermal denaturation data were performed using GraphPad Prism (GraphPad Software, Inc.) by constraining the shared value of slope for all the data sets. Statistical analysis was done in Origin (OriginLab). Significance between binding constants was tested using a Z-test for the two population means,

$$Z = \frac{(\bar{X}_1 - \bar{X}_2)}{(\sigma_1^2 + \sigma_2^2)} \qquad \text{(Eq. 3)}$$

where X_1 and X_2 are the two binding constants, and σ_1 and σ_2 are their standard deviations. p values were Bonferroni corrected (***, $p < 0.001$; **, $p < 0.01$; *, $p < 0.05$).

Far-Western blot

The interaction between AQP2 and LIP5 and its dependence on C-terminal truncation and phosphorylation was studied using far-Western blot as described by Wu *et al.* (33). Human AQP4 was used as negative control. 5 μg of each protein was run on an SDS-PAGE gel and transferred to a nitrocellulose membrane. The membrane was subjected to four subsequent 30-min incubation steps in buffer (20 mM Tris, pH 7.6, 100 mM NaCl) containing 6, 3, 1, and 0.1 M guanidine hydrochloride, followed by a final incubation for 1 h in the same buffer without guanidine hydrochloride. This allows the transferred proteins to denature and then re-nature. The membrane was blocked with 5% (w/v) milk in PBST for 1 h at room temperature followed by overnight incubation at 4 °C with interacting protein LIP5 (0.5 μg/ml). The membrane was washed with PBST buffer three times for 10 min each to remove unbound LIP5, after which it was incubated with an rabbit anti-mouse LIP5 antibody (20) diluted 1:2000 in PBST containing 3% (w/v) milk for 1 h at room temperature. After washing for 3 × 10 mins in PBST as above, the membrane was incubated with a secondary antibody (HRP anti-rabbit IgG, 374-1507; Kirkegaard and Perry Laboratories) diluted 1:1500 dilution in PBST containing 3% (w/v) milk 1 h at room temperature. Finally, the membrane was washed for 3 × 10 min in PBST followed by a single rinse of 5 min with PBS buffer and developed using ECL chemiluminescence (GE Healthcare).

Prior to the incubation with LIP5, loading of protein equivalents and equal protein transfer to the blotting membrane was confirmed by staining with Ponceau reagent, as well as antibodies against the His tag. For Ponceau staining, the membrane was incubated in Ponceau S solution (Sigma-Aldrich) for 5 min, after which the stain was removed by washing in Milli Q water.

For staining with antibodies against the His tag, the membrane was incubated with anti-His antibody (His$_6$ monoclonal antibody, 631212 (albumin-free); Clontech), diluted 1:5000 in 3% milk in PBST for 1 h. After washing for 3×10 min each, the membrane was incubated with a secondary antibody (anti-mouse IgG, 374-1806; Kirkegaard and Perry Laboratories) diluted 1:5000 in 3% milk in PBST for 1 h. The membrane was washed three times for 10 min in PBST followed by a 5-min wash with PBS and developed using ECL chemiluminescence.

Quantification of far-Western blot signal

The far-Western blot signal from three individual blots was quantified using the gel analysis software Gene Tools from Syngene (Synoptics Ltd.). The blots were quantified by manual band quantification using the image type absorption. For each band, an equally sized area was used for quantification, and the background was subtracted using the inbuilt option in the software. All intensities were within the linear range. For each blot, the signal for wild-type AQP2 was set to 100% and the relative signal for all other samples was determined. The data were further analyzed in Origin (Origin Lab Corporation) by one-way analysis of variance to calculate the mean and standard deviation and a p-test to explore the statistical significance.

Microscale thermophoresis

For MST experiments using full-WT-AQP2, AQP2 mutants and AQP4, LIP5 was fluorescently labeled with the amine-reactive dye (NT-647-NHS) using the Monolith™ protein labeling kit RED-NHS (NanoTemper Technologies) according to the manufacturer's instructions. Prior to labeling, the LIP5 buffer was exchanged to the labeling buffer supplied by the kit. After labeling, the protein was eluted into buffer A (20 mM Tris, pH 8, 300 mM NaCl, 0.2% OGNPG), which was also used as assay buffer for MST experiments. Dephosphorylated wild-type AQP2 (3 μM), AQP2–256E (30 μM), AQP2-S261E (30 μM), AQP2-S264E (30 μM), AQP2-T269E (15 μM), and AQP2-S256E/T269E (60 μM) mutants was titrated in a 2:1 dilution series resulting in 16 different samples. For AQP2-ΔP242 (240) μM and AQP4 (100 μM), a 1:1 dilution series was employed. Starting concentrations are given in parentheses. Each sample was diluted 2-fold with a solution containing labeled LIP5 at a concentration of 90 nM (wild-type AQP2, AQP2-ΔP242, AQP2-S256E/T269E, and AQP4), 30 nM (AQP2-T269E), or 60 nM (AQP2-S256E, AQP2-S261E, and AQP264E). The samples were transferred to Monolith™ NT.115 MST premium coated capillaries (NanoTemper Technologies), and MST traces were recorded at room temperature in a Monolith NT.115 (NanoTemper Technologies) using the MO.Control software (LED/excitation power setting 20, MST power setting 40). For all proteins, MST data were obtained from three individually prepared dilution series. The data were analyzed using Origin.

For the peptide binding experiments, peptides corresponding to residues 244–271 in its unphosphorylated state and singly phosphorylated at Ser[256], Ser[261], Ser[264], and Thr[269] were purchased from GenScript. Peptide interactions with AQP2 itself was probed using full-length AQP2 that had been labeled with Alexa Fluor 488 C5-maleimide (Thermo Scientific), according to the manufacturer's instructions, overnight at 4 °C

in 20 mM Tris-HCl, 300 mM NaCl, 0.2% OGNPG, pH 7.4. Excess dye was removed using a PD-10 column. A 1.5-fold dilution series of phosphorylated peptides (10 μM) was made, resulting in 16 samples that were mixed 1:1 with labeled AQP2. The final concentration of AQP2 was 500 nM in all samples. For binding experiments against LIP5, a 2-fold dilution series of unphosphorylated and phosphorylated peptides (20 μM) was made and mixed with LIP5 that had been labeled as described for MST experiments with wild-type AQP2 and AQP2 mutants. MST traces were recorded as described above using a LED/excitation power setting of 40 and MST power setting of 60 for experiments against labeled AQP2. For experiments against labeled LIP5 the LED/excitation power settings and MST power setting was 20 and 60, respectively. All experiments were measured in triplicate.

MST data analysis

The MST-data could be fitted to a one-to-one state binding model using the following equations,

$$y = S_1 + (S_2 - S_1)\left(\frac{L_{\text{Free}}}{L_{\text{Free}} + K_d}\right) \qquad \text{(Eq. 4)}$$

$$L_{\text{Free}} = 0.5(L_{\text{Tot}} - P_{\text{Tot}} - K_d) + \sqrt{(K_d + P_{\text{Tot}} - L_{\text{Tot}})^2 + L_{\text{Tot}}K_d}$$

(Eq. 5)

where S_1 is the signal from the unbound state, and S_2 the signal from the complex; L_{Free} and L_{Tot} are the free and total monomeric [AQP2] concentration, respectively; P_{Tot} is the total concentration of fluorescently labeled LIP5, and K_d is the dissociation constant. Fitting was performed in Origin. Significance between K_d values was tested using a Z-test for two population means as described under CD data analysis above. Linear regression analysis for the correlation between $\log K_d$ and $1/T_{\text{M}}$ was carried out in GraphPad Prism (GraphPad Software, Inc.), giving a slope of 5079 ± 2883 and an $R^2 = 0.4369$.

References

1. Pearce, D., Soundararajan, R., Trimpert, C., Kashlan, O. B., Deen, P. M., and Kohan, D. E. (2015) Collecting duct principal cell transport processes and their regulation. *Clin. J. Am. Soc. Nephrol.* **10,** 135–146

2. Fushimi, K., Sasaki, S., and Marumo, F. (1997) Phosphorylation of serine 256 is required for cAMP-dependent regulatory exocytosis of the aquaporin-2 water channel. *J. Biol. Chem.* **272,** 14800–14804

3. Katsura, T., Gustafson, C. E., Ausiello, D. A., and Brown, D. (1997) Protein kinase A phosphorylation is involved in regulated exocytosis of aquaporin-2 in transfected LLC-PK1 cells. *Am. J. Physiol.* **272,** F817–F822

4. van Balkom, B. W., Savelkoul, P. J., Markovich, D., Hofman, E., Nielsen, S., van der Sluijs, P., and Deen, P. M. (2002) The role of putative phosphory-

lation sites in the targeting and shuttling of the aquaporin-2 water channel. *J. Biol. Chem.* **277,** 41473–41479

5. Kamsteeg, E. J., Hendriks, G., Boone, M., Konings, I. B., Oorschot, V., van der Sluijs, P., Klumperman, J., and Deen, P. M. (2006) Short-chain ubiquitination mediates the regulated endocytosis of the aquaporin-2 water channel. *Proc. Natl. Acad. Sci. U.S.A.* **103,** 18344–18349

6. Pisitkun, T., Shen, R. F., and Knepper, M. A. (2004) Identification and proteomic profiling of exosomes in human urine. *Proc. Natl. Acad. Sci. U.S.A.* **101,** 13368–13373

7. Fenton, R. A., Moeller, H. B., Hoffert, J. D., Yu, M. J., Nielsen, S., and Knepper, M. A. (2008) Acute regulation of aquaporin-2 phosphorylation at Ser-264 by vasopressin. *Proc. Natl. Acad. Sci. U.S.A.* **105,** 3134–3139

8. Hoffert, J. D., Fenton, R. A., Moeller, H. B., Simons, B., Tchapyjnikov, D., McDill, B. W., Yu, M. J., Pisitkun, T., Chen, F., and Knepper, M. A. (2008) Vasopressin-stimulated increase in phosphorylation at Ser[269] potentiates plasma membrane retention of aquaporin-2. *J. Biol. Chem.* **283,** 24617–24627

9. Hoffert, J. D., Nielsen, J., Yu, M. J., Pisitkun, T., Schleicher, S. M., Nielsen, S., and Knepper, M. A. (2007) Dynamics of aquaporin-2 serine-261 phosphorylation in response to short-term vasopressin treatment in collecting duct. *Am. J. Physiol. Renal Physiol.* **292,** F691–F700

10. Moeller, H. B., Aroankins, T. S., Slengerik-Hansen, J., Pisitkun, T., and Fenton, R. A. (2014) Phosphorylation and ubiquitylation are opposing processes that regulate endocytosis of the water channel aquaporin-2. *J. Cell Sci.* **127,** 3174–3183

11. Moeller, H. B., Praetorius, J., Rützler, M. R., and Fenton, R. A. (2010) Phosphorylation of aquaporin-2 regulates its endocytosis and protein-protein interactions. *Proc. Natl. Acad. Sci. U.S.A.* **107,** 424–429

12. Moeller, H. B., MacAulay, N., Knepper, M. A., and Fenton, R. A. (2009) Role of multiple phosphorylation sites in the COOH-terminal tail of aquaporin-2 for water transport: evidence against channel gating. *Am. J. Physiol. Renal Physiol.* **296,** F649–F657

13. Tamma, G., Robben, J. H., Trimpert, C., Boone, M., and Deen, P. M. (2011) Regulation of AQP2 localization by S256 and S261 phosphorylation and ubiquitination. *Am. J. Physiol. Cell Physiol.* **300,** C636–C646

14. Derby, M. C., and Gleeson, P. A. (2007) New insights into membrane trafficking and protein sorting. *Int. Rev. Cytol.* **261,** 47–116

15. Mellman, I., and Nelson, W. J. (2008) Coordinated protein sorting, targeting and distribution in polarized cells. *Nat. Rev. Mol. Cell Biol.* **9,** 833–845

16. Lu, H. A., Sun, T. X., Matsuzaki, T., Yi, X. H., Eswara, J., Bouley, R., McKee, M., and Brown, D. (2007) Heat shock protein 70 interacts with aquaporin-2 and regulates its trafficking. *J. Biol. Chem.* **282,** 28721–28732

17. Park, E. J., Lim, J. S., Jung, H. J., Kim, E., Han, K. H., and Kwon, T. H. (2013) The role of 70-kDa heat shock protein in dDAVP-induced AQP2 trafficking in kidney collecting duct cells. *Am. J. Physiol. Renal Physiol.* **304,** F958–F971

18. Tamma, G., Procino, G., Mola, M. G., Svelto, M., and Valenti, G. (2008) Functional involvement of Annexin-2 in cAMP induced AQP2 trafficking. *Pflugers Arch.* **456,** 729–736

19. Noda, Y., Horikawa, S., Furukawa, T., Hirai, K., Katayama, Y., Asai, T., Kuwahara, M., Katagiri, K., Kinashi, T., Hattori, M., Minato, N., and Sasaki, S. (2004) Aquaporin-2 trafficking is regulated by PDZ-domain containing protein SPA-1. *FEBS Lett.* **568,** 139–145

20. van Balkom, B. W., Boone, M., Hendriks, G., Kamsteeg, E. J., Robben, J. H., Stronks, H. C., van der Voorde, A., van Herp, F., van der Sluijs, P., and Deen, P. M. (2009) LIP5 interacts with aquaporin 2 and facilitates its lysosomal degradation. *J. Am. Soc. Nephrol.* **20,** 990–1001

21. Moeller, H. B., Slengerik-Hansen, J., Aroankins, T., Assentoft, M., MacAulay, N., Moestrup, S. K., Bhalla, V., and Fenton, R. A. (2016) Regulation of the Water Channel Aquaporin-2 via 14-3-3θ and -ζ. *J. Biol. Chem.* **291,** 2469–2484

22. Zwang, N. A., Hoffert, J. D., Pisitkun, T., Moeller, H. B., Fenton, R. A., and Knepper, M. A. (2009) Identification of phosphorylation-dependent binding partners of aquaporin-2 using protein mass spectrometry. *J. Proteome Res.* **8,** 1540–1554

23. Skalicky, J. J., Arii, J., Wenzel, D. M., Stubblefield, W. M., Katsuyama, A., Uter, N. T., Bajorek, M., Myszka, D. G., and Sundquist, W. I. (2012) Interactions of the human LIP5 regulatory protein with endosomal sorting complexes required for transport. *J. Biol. Chem.* **287,** 43910–43926

24. Vild, C. J., Li, Y., Guo, E. Z., Liu, Y., and Xu, Z. (2015) A novel mechanism of regulating the ATPase VPS4 by its cofactor LIP5 and the endosomal sorting complex required for transport (ESCRT)-III protein CHMP5. *J. Biol. Chem.* **290,** 7291–7303

25. Yang, D., and Hurley, J. H. (2010) Structural role of the Vps4-Vta1 interface in ESCRT-III recycling. *Structure* **18,** 976–984

26. Frick, A., Eriksson, U. K., de Mattia, F., Oberg, F., Hedfalk, K., Neutze, R., de Grip, W. J., Deen, P. M., and Törnroth-Horsefield, S. (2014) X-ray structure of human aquaporin 2 and its implications for nephrogenic diabetes insipidus and trafficking. *Proc. Natl. Acad. Sci. U.S.A.* **111,** 6305–6310

27. Dephoure, N., Gould, K. L., Gygi, S. P., and Kellogg, D. R. (2013) Mapping and analysis of phosphorylation sites: a quick guide for cell biologists. *Mol. Biol. Cell* **24,** 535–542

28. Ampah-Korsah, H., Anderberg, H. I., Engfors, A., Kirscht, A., Norden, K., Kjellstrom, S., Kjellbom, P., and Johanson, U. (2016) The aquaporin splice variant NbXIP1;1α is permeable to boric acid and is phosphorylated in the N-terminal domain. *Front. Plant Sci.* **7,** 862

29. Rath, A., Glibowicka, M., Nadeau, V. G., Chen, G., and Deber, C. M. (2009) Detergent binding explains anomalous SDS-PAGE migration of membrane proteins. *Proc. Natl. Acad. Sci. U.S.A.* **106,** 1760–1765

30. Hoffert, J. D., Pisitkun, T., Wang, G., Shen, R. F., and Knepper, M. A. (2006) Quantitative phosphoproteomics of vasopressin-sensitive renal cells: regulation of aquaporin-2 phosphorylation at two sites. *Proc. Natl. Acad. Sci. U.S.A.* **103,** 7159–7164

31. Hoffert, J. D., Wang, G., Pisitkun, T., Shen, R. F., and Knepper, M. A. (2007) An automated platform for analysis of phosphoproteomic datasets: application to kidney collecting duct phosphoproteins. *J. Proteome Res.* **6,** 3501–3508

32. Arthur, J., Huang, J., Nomura, N., Jin, W. W., Li, W., Cheng, X., Brown, D., and Lu, H. J. (2015) Characterization of the putative phosphorylation sites of the AQP2 C terminus and their role in AQP2 trafficking in LLC-PK1 cells. *Am. J. Physiol. Renal Physiol* **309,** F673–F679

33. Wu, Y., Li, Q., and Chen, X. Z. (2007) Detecting protein-protein interactions by Far western blotting. *Nat. Protoc.* **2,** 3278–3284

34. Guo, E. Z., and Xu, Z. (2015) Distinct mechanisms of recognizing endosomal sorting complex required for transport III (ESCRT-III) protein IST1 by different microtubule interacting and trafficking (MIT) domains. *J. Biol. Chem.* **290,** 8396–8408

35. Tseng, W. C., Lin, J. W., Wei, T. Y., and Fang, T. Y. (2008) A novel megaprimed and ligase-free, PCR-based, site-directed mutagenesis method. *Anal. Biochem.* **375,** 376–378

36. Kinoshita, E., Kinoshita-Kikuta, E., Sugiyama, Y., Fukada, Y., Ozeki, T., and Koike, T. (2012) Highly sensitive detection of protein phosphorylation by using improved Phos-tag biotin. *Proteomics* **12,** 932–937

37. Wiśniewski, J. R., Zougman, A., Nagaraj, N., and Mann, M. (2009) Universal sample preparation method for proteome analysis. *Nat. Methods* **6,** 359–362

ASBMB

Phosphorylation of human aquaporin 2 (AQP2) allosterically controls its interaction with the lysosomal trafficking protein LIP5

Jennifer Virginia Roche, Sabeen Survery, Stefan Kreida, Veronika Nesverova, Henry Ampah-Korsah, Maria Gourdon, Peter M. T. Deen and Susanna Törnroth-Horsefield

Access the most updated version of this article at doi: 10.1074/jbc.M117.788364

Alerts:
- When this article is cited
- When a correction for this article is posted

Click here to choose from all of JBC's e-mail alerts

Supplemental material:
http://www.jbc.org/content/suppl/2017/07/14/M117.788364.DC1

This article cites 37 references, 24 of which can be accessed free at
http://www.jbc.org/content/292/35/14636.full.html#ref-list-1